THE JOURNAL OF BIOLOGICAL CHEMISTRY VOL. 283, NO. 16, pp. 10930–10938, April 18, 2008

Decreasing Intracellular Superoxide Corrects Defective Ischemia-induced New Vessel Formation in Diabetic Mice*

Received for publication, September 5, 2007, and in revised form, January 7, 2008 Published, JBC Papers in Press, January 28, 2008, DOI 10.1074/jbc.M707451200

Daniel J. Ceradini[‡1], Dachun Yao[§1], Raymon H. Grogan[‡], Matthew J. Callaghan[‡], Diane Edelstein[§], Michael Brownlee[§2], and Geoffrey C. Gurtner[‡]

From the [‡]Department of Surgery, Stanford University School of Medicine, Stanford, California 94305-5148 and the [§]JDRF International Center for Diabetic Complications Research, Albert Einstein College of Medicine, Bronx, New York 10461-1602

Tissue ischemia promotes vasculogenesis through chemokine-induced recruitment of bone marrow-derived endothelial progenitor cells (EPCs). Diabetes significantly impairs this process. Because hyperglycemia increases reactive oxygen species in a number of cell types, and because many of the defects responsible for impaired vasculogenesis involve HIF1-regulated genes, we hypothesized that HIF1 function is impaired in diabetes because of reactive oxygen species-induced modification of HIF1α by the glyoxalase 1 (GLO1) substrate methylglyoxal. Decreasing superoxide in diabetic mice by either transgenic expression of manganese superoxide dismutase or by administration of an superoxide dismutase mimetic corrected post-ischemic defects in neovascularization, oxygen delivery, and chemokine expression, and normalized tissue survival. In hypoxic fibroblasts cultured in high glucose, overexpression of GLO1 prevented reduced expression of both the EPC mobilizing chemokine stromal cell-derived factor-1 (SDF-1) and of vascular epidermal growth factor, which modulates growth and differentiation of recruited EPCs. In hypoxic EPCs cultured in high glucose, overexpression of GLO1 prevented reduced expression of both the SDF-1 receptor CXCR4, and endothelial nitric-oxide synthase, an enzyme essential for EPC mobilization. HIF1α modification by methylglyoxal reduced heterodimer formation and HIF1α binding to all relevant promoters. These results provide a basis for the rational design of new therapeutics to normalize impaired ischemia-induced vasculogenesis in patients with diabetes.

Studies in both experimental animals and humans have shown that diabetes impairs ischemia-driven neovascularization (1, 2). Diabetic animals have a decreased vascular density following hind limb ischemia (3, 4) and impaired wound healing (5). Human angiograms demonstrate fewer collateral vessels in diabetic patients compared with non-diabetic controls (1). Clinically, this contributes to increased rates of lower limb amputation, heart failure, and increased mortality after ischemic events.

Ischemic tissue selectively recruits endothelial progenitor cells (EPCs)[3] from the bone marrow compartment by up-regulating the chemokine stromal cell-derived factor-1 (SDF-1). SDF-1 expression acts as a signal indicating the presence of tissue ischemia, and its expression is directly regulated by hypoxia-inducible factor-1 (5, 6). Ischemic tissue also up-regulates expression of VEGF, which modulates growth and differentiation of recruited EPCs (7). Endothelial cell mobilization from the bone marrow compartment is mediated by the SDF-1 receptor CXCR4, and endothelial nitric-oxide synthase plays an essential role in this mobilization (8). In diabetic mice, expression of SDF-1 in peripheral wound tissue is decreased, and in diabetic mice and humans, there is a significant decrease in circulating EPCs (5, 9), which exhibit impaired proliferation, adhesion, and incorporation into vascular structures (9). The mechanisms underlying defective ischemia-induced vasculogenesis in diabetes remain unclear.

One common element in the different environments where vasculogenesis is believed to occur in the presence of a hypoxic stimulus (10). Hypoxia-inducible gene transcription is normally regulated by hypoxia-inducible factor 1 (HIF-1), a heterodimeric master regulator of hypoxia-inducible gene transcription (11) composed of an α subunit, HIF-1α, which is labile in the presence of oxygen, and a constitutively expressed stable β subunit, aryl hydrocarbon receptor nuclear translocator (ARNT). In the presence of normal oxygen concentrations, HIF-1α is hydroxylated at two conserved proline residues, ubiquinated, and then degraded by the proteosome. This process is mediated by the von Hippel-Lindau tumor suppressor protein, which binds to hydroxylated HIF-1α. When oxygen concentration is low, hydroxylation does not occur, allowing HIF-1α protein levels to rise. The HIF-1α/ARNT heterodimer then binds to a consensus hypoxia response element (HRE), where it recruits the coactivator p300/CREB-binding protein and activates transcription. Because HIF1α regulates transcription of SDF-1, VEGF, CXCR4, and endothelial nitric-oxide synthase (eNOS) in response to hypoxia, and because the bone

* This work was supported by NIDDK, National Institutes of Health Grants R01 DK74153-01 (to M. B.) and R01 DK74095-01 (to G. G.). The costs of publication of this article were defrayed in part by the payment of page charges. This article must therefore be hereby marked "*advertisement*" in accordance with 18 U.S.C. Section 1734 solely to indicate this fact.

[1] Both authors contributed equally to the work.

[2] To whom correspondence should be addressed: F-531, 1300 Morris Park Ave., Bronx NY 10461. Tel.: 718-430-3636; Fax: 718-430-8570; E-mail: brownlee@aecom.yu.edu.

[3] The abbreviations used are: EPCs, endothelial progenitor cells; ARNT, aryl hydrocarbon receptor nuclear translocator; ChIP, chromatin immunoprecipitation; eNOS, endothelial nitric-oxide synthase; GLO1, glyoxalase 1; HIF1α, hypoxia-inducible factor-1α; MG, methylglyoxal; Mn-SOD, manganese superoxide dismutase; ROS, reactive oxygen species; SDF1, stromal cell-derived factor-1; VEGF, vascular endothelial growth factor; qPCR, quantitative PCR; HRE, hypoxia response element; CREB, cAMP-response element-binding protein; Mn-TBAP, manganese(III) meso-tetrakis(4-carboxyphenyl)porphyrin; GAPDH, glyceraldehyde-3-phosphate dehydrogenase; WT, wild type; bHLH, basic helix loop helix.

marrow niche is normally hypoxic, we hypothesized that a diabetes-induced defect in HIF1α could cause both defective cell signaling in response to ischemia, and defective EPC response to those signals.

Hyperglycemia increases reactive oxygen species (ROS) in cell types affected by diabetic complications, and these ROS initiate several complex series of molecular events that result in diabetic tissue damage (12). In non-diabetic glutathione peroxidase 1-deficient mice, increased ROS causes impaired revascularization in the ischemic hindlimb model, accompanied by impaired EPC mobilization and function (13). One consequence of increased intracellular ROS is accumulation of the highly reactive dicarbonyl methylglyoxal, a degradation product formed from triose phosphates during glycolysis, which forms stable adducts primarily with arginine residues of intracellular proteins. Because high glucose and diabetes increase angiopoietin-2 transcription in endothelial cells through methylglyoxal modification of the corepressor mSin3A (14), we further postulated that this consequence of increased ROS affects the HIF1-dependent expression of genes involved in ischemia-induced vasculogenesis.

EXPERIMENTAL PROCEDURES

Murine Diabetes and Ischemia Model—Diabetes was induced in 2–4-month old C57Bl/6 mice with streptozotocin, and stable hyperglycemia was confirmed 14 days after treatment with monitoring at regular intervals thereafter. Age-matched non-diabetic littermates served as controls. Three weeks after induction of diabetes, animals began daily treatment with manganese(III) meso-tetrakis(4-carboxyphenyl)porphyrin (Mn-TBAP, 10 mg/kg per day, dissolved in 0.005 M NaOH solution) or carrier (control), which was continued for the duration of the experiments. In parallel, transgenic mice that overexpress *Mn-SOD* (*Mn-SOD*+/−) underwent identical diabetes induction with similar age-matched controls. This formed six experimental groups: non-diabetic wild type, non-diabetic Mn-TBAP-treated, non-diabetic *Mn-SOD* transgenic, diabetic wild type, diabetic Mn-TBAP-treated, and diabetic *Mn-SOD* transgenics. After 4 weeks of diabetes, all animals were used in the mouse ischemia model as previously described in full accordance with the New York University Institutional Animal Care and Use Committee. Briefly, a peninsular shaped incision was made on the dorsum of mice, generating a reproducible gradient of soft tissue ischemia (6, 9). Over the course of 14 days, gene expression, blood flow, tissue oxygenation, mobilization, and recruitment of endothelial progenitors, tissue viability, and neovascularization were assessed. Mouse blood glucose was determined by testing 5 μl of tail vein blood using a One Touch Blood Glucose monitoring system (Life Scan, Johnson and Johnson).

Tissue Perfusion, Oxygen Tension Measurements, and Viability—Blood flow and tissue oxygenation was determined as described previously on postoperative days 7 and 14 (9). An optical fiber probe (100-μm radius, Oxford Optronix) matched with a thermocoupler was directly inserted into tissue, allowing for continuous temperature-compensated oxygen tension measurements (10 values/s). The probe was positioned at each of four reference points (points 1–4) for 60 s, generating an average of 600 values per trial. Perfusion was measured with color laser Doppler (Moor Instruments). Relative blood flow was calculated as previously described (9). Gross tissue viability was determined by digital imaging techniques, and the percentage of clinically viable tissue was calculated using the SigmaScan software package.

Immunohistochemistry—Samples from each ischemic tissue area (A–C) as well as a non-ischemic control (D) were harvested at regular intervals as indicated, and either snap-frozen in liquid nitrogen or embedded in paraffin. Capillary density in each area was determined from five nonconsecutive 10-μm sections using phosphatidylethanolamine-conjugated CD31 immunostaining (Pharmingen) as previously described (9).

Mobilization of Endothelial Progenitor Cells—On postoperative day 7, the number of circulating endothelial progenitor cells was determined by flow cytometry. Following red blood cell lysis with ammonium chloride, whole blood was stained with antibodies for flk-1-PE and CD11b-fluorescein isothiocyanate to identify endothelial progenitor cells as flk-1+/CD11b−, as described previously (15). The mean percentage of circulating EPCs in each experimental group was calculated using four independent experiments.

Bone Marrow Transplant Model—Following sublethal radiation (gray), a group of wild type FVB mice were transplanted with bone marrow harvested from FVB *Tie2*/*LacZ* transgenic mice, which feature the *LacZ* gene driven by the endothelial-specific *Tie2* promoter. In this transplanted group, all newly formed endothelial cells derived from the bone marrow specifically express β-galactosidase, and can be used to readily identify neovascularization that proceeds via endothelial progenitor cells during postnatal vasculogenesis (15). Following reconstitution over 4 weeks, diabetes induction, treatment with Mn-TBAP, and ischemic surgery proceeded as above. Intact tissue was harvested and stained with the β-galactosidase staining kit (Roche), followed by sectioning for histologic analysis. The number of β-galactosidase positive endothelial cells in each tissue area was enumerated in five nonconsecutive sections at $\times$200.

Serum Enzyme-linked Immunosorbent Assay—Enzyme-linked immunosorbent assay was performed using the human/mouse SDF-1 and VEGF Quantikine kit according to the manufacturer's protocol (R&D). Cell culture supernatants were used following standardization of each sample by total protein content using the BCA Protein Assay Kit (Pierce). Results are representative of four independent experiments.

Migration Assays—Migration was studied using a modified transwell assay. Lin−/Sca-1+/c-kit+ (5×10^4) were seeded onto Chemotx filters (5.7-mm, 8-μm pore, Neuro Probe) in endothelial basal medium, 0.5% fetal bovine serum. Recombinant human SDF-1β/pre-β cell growth-stimulating factor (Sigma) was then added to the lower chamber. Following the 6-h migration period, nonmigrating cells were completely wiped from the top surface of the membrane. Migrating cells were quantified using Kodak One-dimensional software. Results are indicative of four independent experiments.

In Vitro Materials—Antibodies for HIF-1α (sc-10790), VEGF (sc-507), SDF-1 (sc-28876), Arnt1 (sc-17811), Gal4-DBD (sc-577), CXCR4 (sc-9046), β-actin (sc-10731, sc-8432), Flt-1

(sc-316), eNOS (sc-653), and Flk-1 (sc-504) were purchased from Santa Cruz Biotechnology. A monoclonal antibody to the major intracellular methylglyoxal-derived epitope, *N*-acetyl-*N*-(5-hydro-5-methyl)-4-imidazolone (MG), was previously generated and characterized by our laboratory (by M. B.). Primary fibroblasts were collected from dorsal skins of either diabetic or wild type mice and maintained in Dulbecco's modified Eagle's medium with 10% fetal bovine serum and antibiotics. Cells were treated with LG (5 mM glucose), HG (30 mM glucose), or HG for 3 days after a 24-h infection with adGLO1. 30 mM L-glucose was used as a negative control. Hypoxia was induced for 18 h prior to analysis in a hypoxic chamber in which O_2 was removed by flushing with 95% CO_2 plus 5% N_2 gas for 15 min. Primary bone marrow cells were collected from the tibia from either diabetic or wild type mice, and maintained in endothelial basal medium with supplements of hydrocortisone, endothelial growth factor, and 10% fetal calf serum on fibronectin/gelatin-coated dishes. The media was refreshed every day for 3 days, and then the cells were stimulated with human recombinant VEGF for 2 days as described previously (16). The adherent cells were characterized by washing with medium and incubating with 2.4 μg/ml 1,1′-dioctadecyl-3,3,3′,3′-tetramethylindocarbocyanine-labeled acetylated low deinsity lipoprotein (Dil-Ac-LDL; Biomedical Technologies Inc., MA) for 1 h. Cells were fixed in 2% paraformaldehyde and counterstained with fluorescein isothiocyanate-labeled lectin from *Ulex europaeus* (Sigma). Double positive staining cells were considered to be EPCs (16). Animal protocols used for these experiments were approved by the Albert Einstein College of Medicine Institutional Animal Care and Use Committee.

Plasmids—For construction of luciferase reporters, murine genomic DNA was purified from primary fibroblasts by DNeasy Tissue Kit (Qiagen), and the *Sdf-1*, *Vegf*, and *Cxcr4* promoters were amplified by PCR. Restriction sites for XhoI and HindIII were introduced, and the fragments were then subcloned into pGL3 basic vector (Promega). For mapping of the HIF-1α-MG modification sites, the murine HIF-1α full-length cDNA or indicated deletions were generated by PCR methods, and the fragments were subcloned into pM vector (Clontech) by introduction of EcoRI and BamHI restriction sites. The indicated single point mutations were generated using the Site-directed Mutagenesis Kit from Promega (Madison, WI). All constructs were verified by sequencing. Detailed information regarding each construct is available upon request. Plasmid DNA was transfected with Lipofectamine™ Reagent (Invitrogen). Luciferase activity assays were carried out using the Dual-Luciferase™ Assay System (Promega) and transfection efficiencies were normalized using a cotransfected *Renilla* plasmid. Nuclear extracts were prepared using the NE-PER Nuclear and Cytoplasmic Extraction Reagents Kit (Pierce). Protein concentration was measured by the Coomassie Protein Assay Kit (Pierce) using bovine serum albumin as a standard.

Immunoprecipitation (IP) and Western Blotting—Cell lysates or nuclear extracts were cleared by preimmune IgG plus Protein A-agarose beads for 2 h, and the supernatants were immunoprecipitated by the indicated antibodies and a 50% slurry of Protein A-agarose beads overnight at 4 °C. After washing with buffer containing 50 mM Tris, pH 7.5, 150 mM NaCl, 1% Nonidet P-40, and 0.5% deoxycholate with protease inhibitors, proteins were released and separated on 10% SDS-PAGE gels. After transfer to membranes, the blots were simultaneously incubated with the differentially labeled species-specific secondary antibodies, anti-rabbit IRDye™ 800CW (green) and anti-mouse Alexa 680 (red). Membranes were scanned and quantitated by the ODYSSEY Infrared Imaging System (LI-COR, NE) and normalized to β-actin.

Chromatin Immunoprecipitation (ChIP)—Treated cells were cross-linked by 1% formaldehyde for 20 min, and terminated by addition of 0.1 M glycine. Cell lysates were sonicated and centrifuged. 500 μg of protein were pre-cleared by bovine serum albumin/salmon sperm DNA plus preimmune IgG and a slurry of Protein A-agarose beads as previously described (17). Immunoprecipitations were performed with the indicated antibodies, bovine serum albumin/salmon sperm DNA, and a 50% slurry of Protein A-agarose beads. Input and immunoprecipitated DNA were washed and eluted, then incubated 2 h at 42 °C in the presence of Proteinase K followed by 6 h at 65 °C to reverse the formaldehyde cross-linking. DNA fragments were recovered by phenol/chloroform extraction and ethanol precipitation. A 150-bp fragment from the murine *Sdf-1*, *Vegf*, *Cxcr4*, and *eNos* promoters were amplified by real-time PCR (qPCR).

Reverse Transcriptase Reaction and Real-time Quantitative PCR—Total RNA from treated cells was extracted using the RNeasy Mini Kit (Qiagen), and the mRNA from ischemic flaps and normal skin was isolated using an RNeasy® Fibrous Tissue Midi Kit (Qiagen, CA). Either the entire peninsular skin flap (ischemic tissue) or a corresponding 1.25 × 2.5-cm segment of skin and soft tissue was harvested and immersed in 2 ml of RLT buffer with β-mercaptoethanol and immediately homogenized and disrupted with a Polytron PT 10-35 (Brinkmann). Total RNA was then isolated per the manufacturer's instructions. The mRNA was reverse transcribed by the SuperScript™ III First Strand Synthesis System (Invitrogen). Real-time quantitative PCR (qPCR) was run on a LightCycler (Roche Molecular Systems) with the LightCycler FastStart DNA Master SYBR Green I kit (Roche). PCR was performed by denaturing at 95 °C for 7 min, followed by 45 cycles of denaturation at 95 °C, annealing at 60 °C, and extension at 72 °C for 10 s, respectively. 1 μl of each cDNA was used to measure target genes, and the results were normalized to β-actin or GAPDH.

Measurement of Reactive Oxygen Species—The levels of superoxide production in primitive bone marrow progenitor cells was determined preoperatively and 14 days following surgery. Bone marrow cells were flushed from the lower extremity long bones with phosphate-buffered saline, 10% fetal calf serum, and lineage depleted using MACS magnetic beads according to the manufacturer's protocol. Lineage-depleted bone marrow was then stained with dihydroethidium (Molecular Probes), c-kit, and Sca-1 antibodies and mean dihydroethidium fluorescence in the Lin−ckit+Sca-1+ population was determined by flow cytometry.

Statistical Analysis—Results are given as mean ± S.D. All experiments were performed at least in triplicate. Data distribution was analyzed, and statistical differences for different treatments were evaluated by analysis of variance and the Tukey-Kramer test using SPSS 15 software.

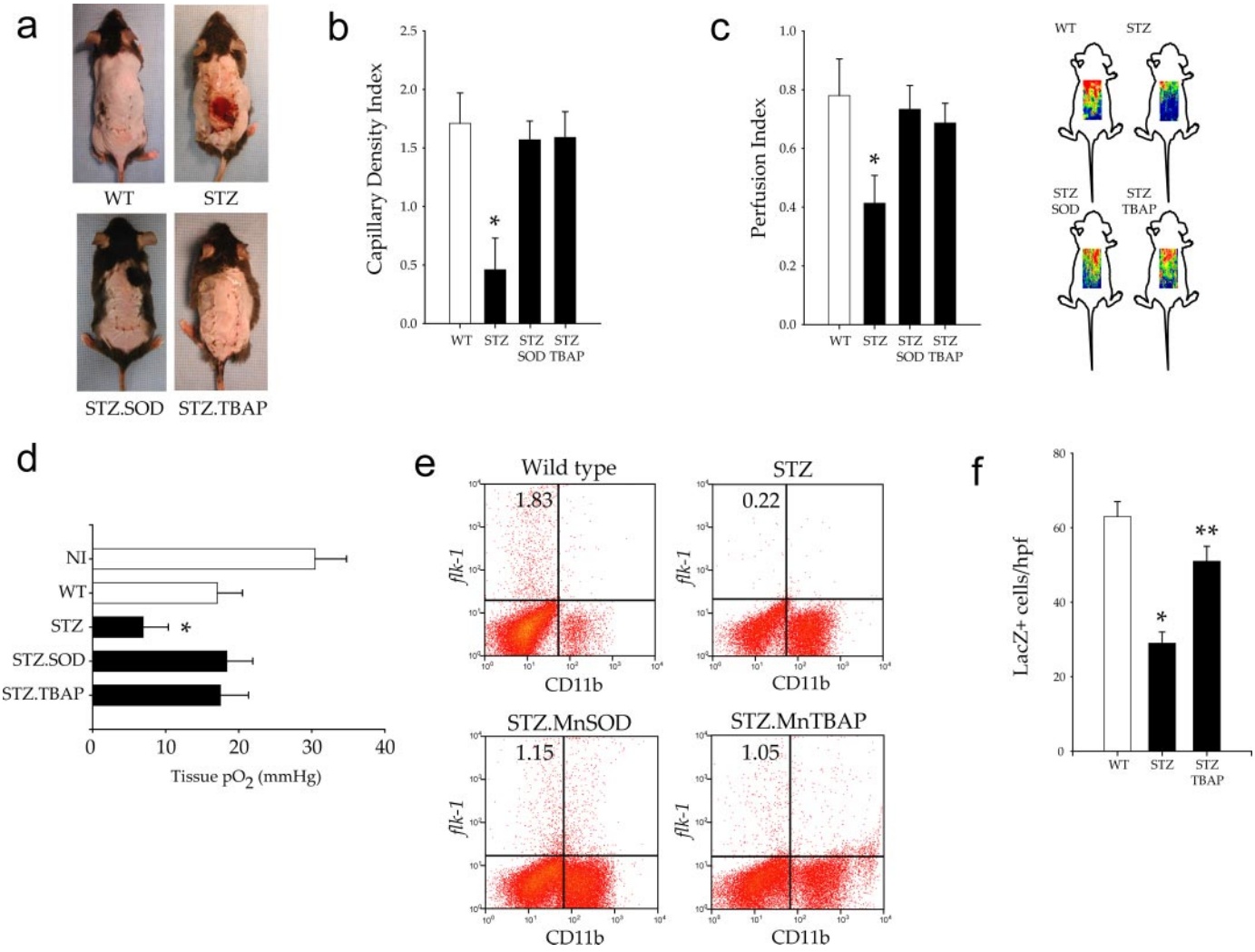

FIGURE 1. **Impaired ischemia-induced vasculogenesis in diabetic mice is corrected both by transgenic expression of *Mn-SOD* and by superoxide dismutase mimetic treatment.** *a*, survival of ischemic tissue assessed at 14–21 days following surgery in wild type, wild type diabetic (*STZ*), diabetic transgenic *Mn-SOD* (*STZ.SOD*), and wild type diabetic mice treated with an SOD mimetic (*STZ.TBAP*). *b* and *c*, capillary density (*b*, *, $p < 0.001$) and relative blood flow quantified by color laser Doppler (*c*, *, $p < 0.01$) 14 days following ischemic surgery. *d*, tissue oxygen tension in normal non-ischemic tissue (*NI*) compared with tissue 7 days following ischemic surgery in each experimental group (*, $p < 0.01$). *e*, mobilization of flk−,+1/CD11b-endothelial progenitor cells 7 days following surgery determined by flow cytometry. *f*, using bone marrow transplantation, the number of lacZ+ bone marrow-derived endothelial cells recruited to new blood vessels after ischemic injury were compared between WT, STZ, and STZ-TBAP mice. *, $p < 0.005$; **, $p < 0.01$. Data are expressed as mean ± S.E., $n = 3$.

RESULTS

Decreasing Intracellular Superoxide Corrects Defective Ischemia-induced New Vessel Formation in Diabetic Mice—We first determined that the most general mechanism underlying our more specific hypothesis, diabetes-induced superoxide production, played a central role in the diabetes defect in ischemia-induced neovascularization, using a previously characterized murine model of soft tissue ischemia. Diabetic mice exhibited a significant impairment in ischemia-induced neovascularization compared with non-diabetic controls, resulting in necrosis of the ischemic soft tissue (Fig. 1*a*, *upper panels*). We evaluated the possible role of diabetes-induced intracellular superoxide formation in defective ischemia-induced neovascularization by using two complementary murine models: diabetic transgenic mice overexpressing manganese superoxide dismutase, the mitochondrial isoform of this enzyme, and diabetic WT mice treated with a cell-permeable superoxide dismutase/catalase mimetic, Mn-TBAP. There was no effect of either the *Mn-SOD* transgene or Mn-TBAP treatment on blood glucose levels in diabetic mice (WT diabetic = 474 + 23 mg/dl, *Mn-SOD* diabetic = 439 + 15 mg/dl, Mn-TBAP diabetic = 508 + 15 mg/dl). In both of these diabetic models, the ischemic soft tissue healed normally (Fig. 1*a*, *lower panels*), and the 70% reduction in ischemic tissue capillary density induced by diabetes was prevented (Fig. 1*b*). Similarly, the 50% reduction in perfusion of the ischemic tissue (Fig. 1*c*) and the resultant decrease in oxygen delivery to the ischemic tissue were also normalized (Fig. 1*d*). Thus, diabetes-induced overproduction of superoxide plays a central role in the pathogenesis of impaired ischemia-induced neovascularization in this disease.

Because humans with diabetes have dramatically reduced levels of circulating EPCs (6), we next determined the level of circulating EPCs mobilized from the bone marrow following an

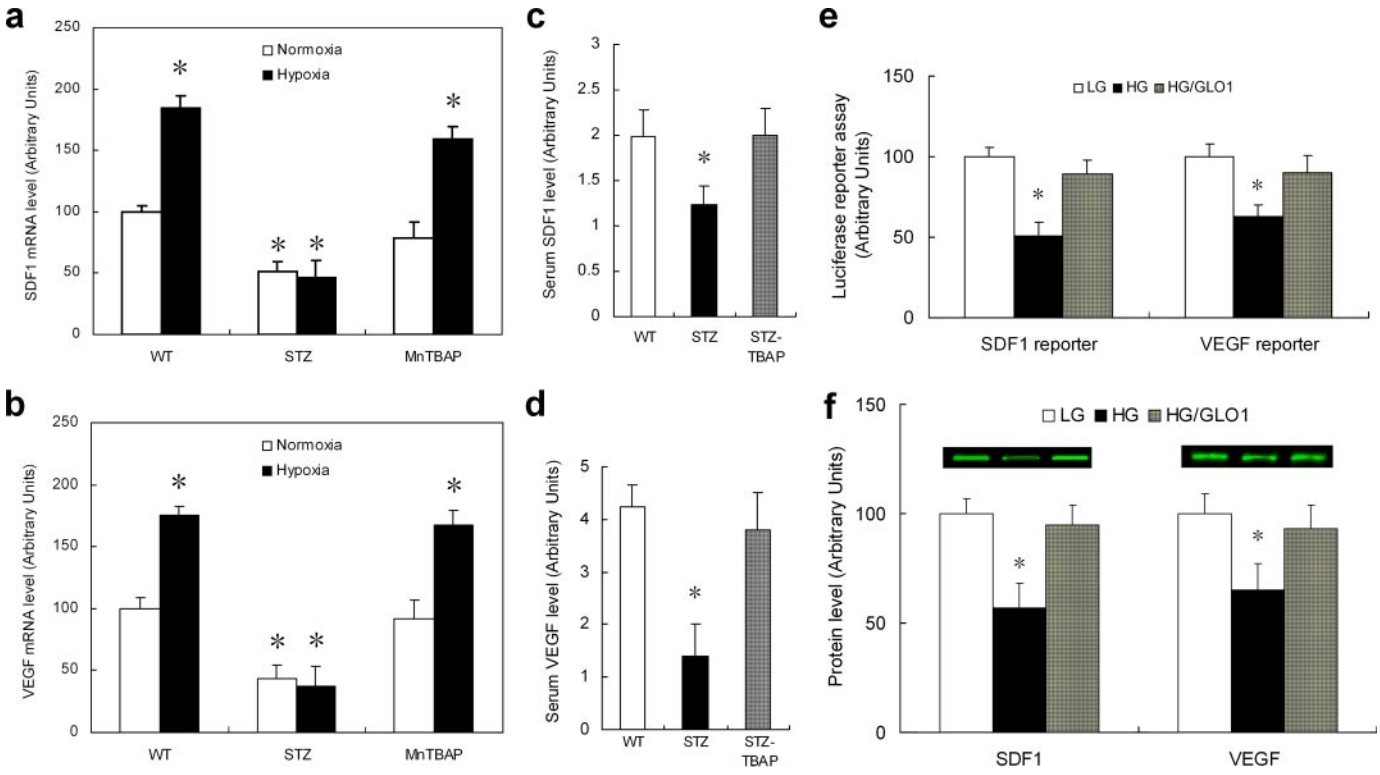

FIGURE 2. **Hypoxia-induced SDF-1 and VEGF expression in fibroblasts was reduced in hyperglycemia.** *a* and *b*, mRNA levels of SDF1 (*a*) and VEGF (*b*) from skin in wild type, wild type diabetic (*STZ*), and wild type diabetic mice treated with an SOD mimetic (*Mn-TBAP*). *, $p < 0.05$ *versus* WT normoxia group. *c* and *d*, protein levels in serum of SDF-1 (*c*) and VEGF (*d*). *, $p < 0.05$ *versus* WT group. *e*, primary fibroblasts isolated from dorsal skin of wild type mice were transfected with SDF-1Luc or VEGFLuc, and incubated under hypoxic conditions in either low glucose (*LG*), high glucose (*HG*), or high glucose following infection with adGLO1 (*HG/GLO1*). Cell lysates were prepared and luciferase activity determined. *, $p < 0.01$ *versus* LG group. *f*, cell lysates were prepared from primary mouse dorsal skin fibroblasts treated as in *e*, and protein levels of SDF-1 and VEGF were determined by Western blotting and quantitated using the ODYSSEY infrared imaging system. *, $p < 0.01$ *versus* LG group. Data are expressed as mean ± S.E., $n = 3$.

ischemic injury in diabetic mice, diabetic *Mn-SOD* transgenic mice, and diabetic mice treated with Mn-TBAP (Fig. 1*e*). Diabetes dramatically reduced the level of mobilized EPCs, to only 12% of levels observed in non-diabetic mice. Notably, this decrease was not attributable to fewer progenitor cells in the bone marrow compartment of diabetic mice, as the number of Lin−/Sca-1+/c-Kit+ progenitor cells (18, 19) from both non-diabetic and diabetic mice was not statistically different. Transgenic expression of Mn-SOD in diabetic mice increased the level of mobilized EPCs to 63% of non-diabetic levels, whereas treatment of diabetics with a SOD mimetic increased the number to 58% of non-diabetic levels. To confirm that the diabetes-induced reduction in mobilized EPCs resulted from a failure to recruit bone marrow-derived EPCs to the site of ischemia, we utilized a transplant model in which bone marrow harvested from *Tie-2/LacZ* mice was transplanted into wild type mice (15, 20). In this model, endothelial cells derived from bone marrow progenitor cells during neovascularization stain β-galactosidase positive. Because the effect of Mn-SOD overexpression and Mn-TBAP treatment were identical (Fig. 1, *a–e*), in this experiment and mouse experiments that followed, only Mn-TBAP-treated diabetic mice were used. Following reconstitution and induction of diabetes, animals underwent ischemic surgery. Prior to surgery, there was no difference in capillary density of diabetics compared with non-diabetics, nor in transplanted diabetics compared with transplanted non-diabetics. However, after surgery, diabetic animals had a greater than 50% reduction in the number of lacZ positive cells recruited to the ischemic tissue (Fig. 1*f*). In contrast, the number of lacZ positive cells recruited in diabetic animals treated with Mn-TBAP was increased 2.2-fold over untreated diabetics, to 77% that observed in non-diabetic mice.

The observed failure of diabetic animals to mobilize and recruit reparative progenitor cells in a peripheral wound model reflects both a failure of the ischemic tissue to generate appropriate levels of at least one chemokine signal, SDF-1α, and a failure of progenitor cells to respond to ischemia-specific signals due in part to a decrease in eNOS activation (5). In our ischemic flap model, diabetic mice showed a significantly blunted up-regulation of SDF-1 mRNA in the ischemic skin flap compared with skin from non-diabetic mice (Fig. 2*a*). Treatment of diabetic mice with the SOD mimetic Mn-TBAP restored SDF-1 mRNA levels in the ischemic skin flap to normal (Fig. 2*a*). VEGF is also thought to mobilize EPCs, and to act locally to modulate growth and differentiation of recruited EPCs (15). In our ischemic flap model, diabetic mice also showed a significantly blunted up-regulation of VEGF mRNA in the ischemic skin flap compared with skin from non-diabetic mice (Fig. 2*b*). Treatment of diabetic mice with the SOD mimetic Mn-TBAP restored VEGF mRNA levels in the ischemic skin flap to normal (Fig. 2*b*). Serum levels of SDF1 and VEGF were both significantly reduced 7 days after ischemic surgery, when progenitor mobilization typically begins to peak (15) (Fig. 2, *c* and *d*). As with skin mRNA levels, reduced serum

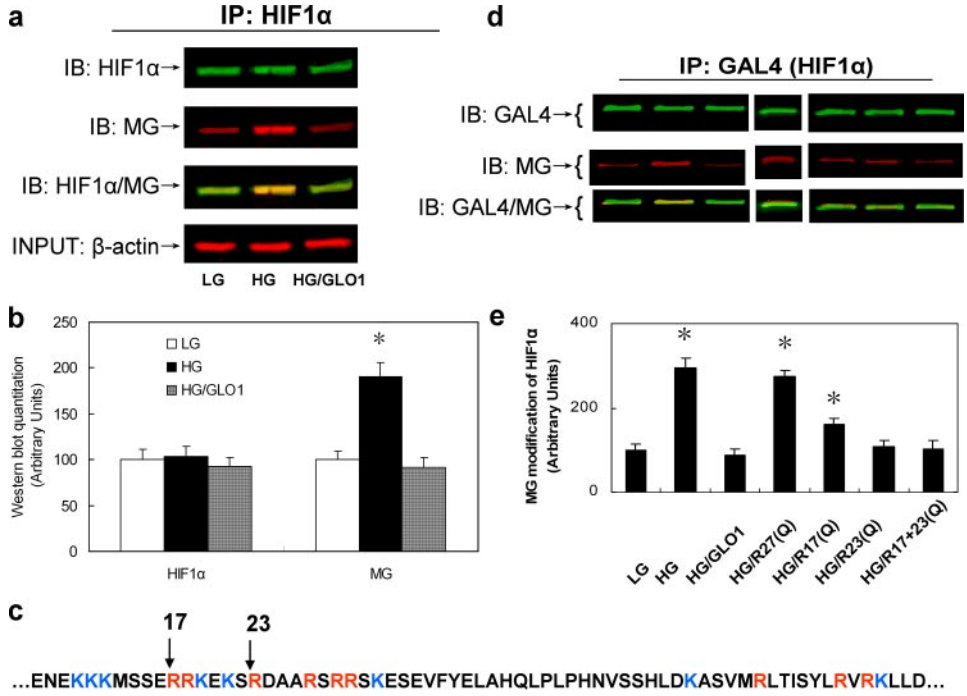

FIGURE 3. **Hyperglycemia-induced methylglyoxal modification of HIF-1α in hypoxic mouse dermal fibroblasts.** *a*, nuclear extracts were isolated from primary mouse dermal fibroblasts and treated as described in the legend to Fig. 2*e*. The extracts were immunoprecipitated (*IP*) with HIF-1α rabbit antibody and then immunoblotted (*IB*) with either HIF-1α antibody, or a monoclonal antibody to the major intracellular methylglyoxal-derived epitope, *N*α-acetyl-*N*δ-(5-hydro-5-methyl)-4-imidazolone (*MG*). *b*, quantitation of methylgloxal modification of HIF1-α in *a*. *c*, amino acid sequence of the murine HIF-1α bHLH domain (AA1–71). Potential MG-reactive arginine and lysine residues are indicated in *red* and *blue*, respectively. *d*, primary mouse dermal fibroblasts were transfected with either full-length GAL4 murine HIF-1α (*LG* and *HG*), GAL4 murine HIF-1α with a R17Q point mutation, GAL4 murine HIF-1α with a R23Q point mutation, GAL4 murine HIF-1α with a R27Q point mutation, or GAL4 murine HIF-1α with both R17Q and R23Q point mutations, and incubated under hypoxic conditions. IP-Western blotting using a Gal4-binding domain rabbit antibody and a monoclonal antibody to the major methylglyoxal-derived epitope was performed as described above. *e*, quantitation of MG modification of HIF1α in *d*. *, $p < 0.01$ *versus* LG group. Data are expressed as mean ± S.E., $n = 3$.

levels of SDF-1 and VEGF in diabetic mice were both restored to normal by treatment of diabetic mice with Mn-TBAP (Fig. 2, *c* and *d*).

Superoxide-induced Methylglyoxal Modification of HIF-1α by High Glucose Causes Defective Fibroblast Signaling in Response to Hypoxia—To understand the molecular mechanisms by which diabetes-induced overproduction of superoxide reduced serum levels of SDF-1 and VEGF, we examined the effect of hyperglycemia on both SDF-1 and VEGF mRNA expression and on secreted protein levels in hypoxic mouse fibroblasts. Fibroblasts were chosen because primary fibroblasts can be easily isolated from murine and human biopsies, and have been the major cell type studied in published HIF-1 research.

Because one significant downstream consequence of hyperglycemia-induced superoxide production is an increase in the intracellular concentration of the highly reactive dicarbonyl methylglyoxal, which can covalently modify intracellular proteins and alter their function (12, 21), we also examined the effect of reducing intracellular methylglyoxal concentrations by glyoxalase 1 overexpression (GLO1) on SDF-1 and VEGF expression in hyperglycemic mouse fibroblasts exposed to hypoxia (Fig. 2, *c* and *d*). Hyperglycemia reduced luciferase reporter expression of both SDF-1 (49%) and VEGF (by 37%) in hypoxic fibroblasts (Fig. 2*e*). These reductions were completely prevented by overexpressing the rate-limiting enzyme of methylglyoxal catabolism, glyoxalase I (GLO1). Similarly, hyperglycemia reduced levels of SDF-1 and VEGF protein secreted by hypoxic fibroblasts by 43 and 36%, respectively (Fig. 2*f*). These defects were also completely prevented by overexpression of GLO1. In contrast, high glucose alone or with GLO1 overexpression did not affect levels of another secreted fibroblast secreted protein, BMP2, suggesting that the observed effects did not reflect a general effect on secretion (data not shown).

Because hypoxia-induced up-regulation of SDF-1 and VEGF expression are both mediated by the transcription factor HIF-1, we hypothesized that hyperglycemia-induced methylglyoxal modification was interfering with some aspect of HIF-1 function. Under hyperglycemic conditions at hypoxic oxygen levels, we found a 1.9-fold increase in modification of HIF-1α protein by methylglyoxal, which was prevented by GLO1 overexpression (Fig. 3, *a* and *b*). ARNT1 was not modified by methylglyoxal (data not shown).

HIF-1α is a member of the basic helix-loop-helix Per/Arnt/Sim (PAS) family, and contains an N-terminal bHLH domain, and a PAS domain, followed by an N-terminal and a C-terminal transactivation domain. Gal4 HIF-1α constructs were made in which each of these domains was deleted, and only the bHLH domain (residues 1–71) showed increased hyperglycemia-induced modification by methylglyoxal (data not shown). Although methylglyoxal reacts primarily with Arg residues *in vivo* to form the major methylglyoxal-derived epitope hydroimidazolone MG-H1 (*N*α-acetyl-*N*δ-(5-hydro-5-methyl)-4-imidazolone) (21), Lys residues in proteins can also be modified (22, 23). We therefore evaluated the possible role of each Arg and Lys residue in the bHLH domain of HIF-1α (Fig. 3*c*) by making point mutants in the bHLH domain that converted each of the 14 residues to glutamine. Mutation of Arg-17 dramatically reduced hyperglycemia-induced methylglyoxal modification of HIF-1α, mutation of Arg-27 did not, whereas mutation of Arg-23 completely prevented hyperglycemia-induced methylglyoxal modification of HIF1α (Fig. 3, *d* and *e*).

The bHLH domain of HIF-1α affects function in two ways: it is critical for heterodimer formation with ARNT, and it is also critical for heterodimer binding to the HRE (24). Hyperglycemia reduced heterodimer formation of HIF-1α with ARNT to 37% of control (Fig. 4, *a* and *b*). This defect was prevented by GLO1 overexpression. Similarly, hyperglycemia reduced

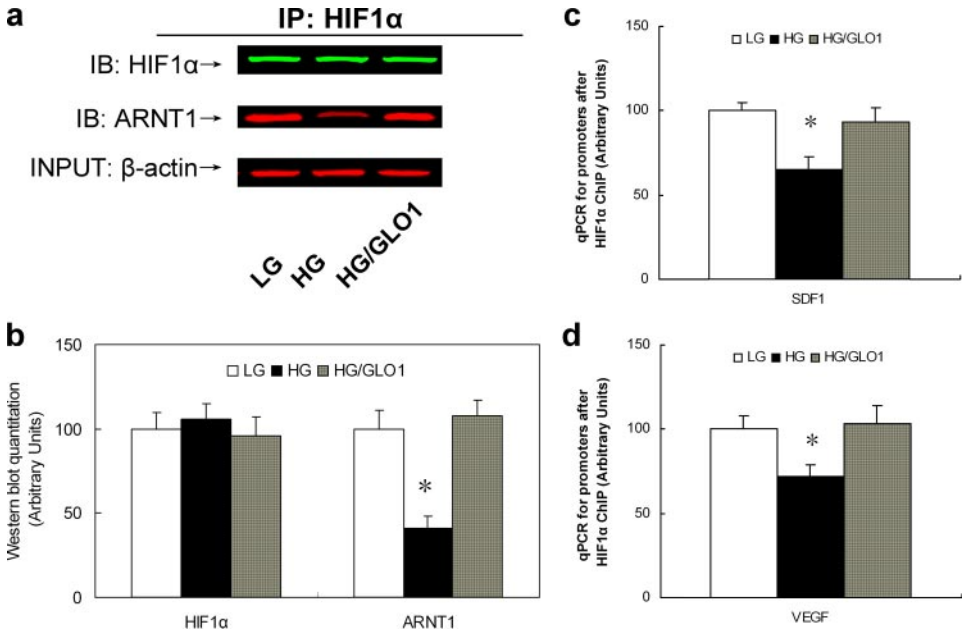

FIGURE 4. **Hyperglycemia-induced methylglyoxal modification of HIF-1α reduces HIF-1 heterodimer formation and HIF-1α binding to the SDF-1 and VEGF promoters in hypoxic mouse dermal fibroblasts.** *a*, nuclear extracts from hypoxic fibroblasts treated as indicated were isolated, immunoprecipitated (*IP*) with HIF-1α rabbit antibody, and immunoblotted (*IB*) with ARNT1 mouse antibody. 10% of nuclear extracts were immunoblotted with β-actin antibody as input control. The membrane was scanned and quantitated by the ODYSSEY Infrared Imaging System. *b*, quantitation of association of HIF1-α with ARNT1 in *a*. *c* and *d*, soluble chromatin was prepared from hypoxic fibroblasts treated as indicated and chromosomal immunoprecipitation was performed using antibody to HIF-1α. The DNA extracted from the respective immunoprecipitates was amplified by real-time PCR (*qPCR*) using primers that cover the SDF-1 (*c*) and VEGF promoters (*d*), respectively. *, $p < 0.01$ *versus* LG group. Data are expressed as mean ± S.E., $n = 3$.

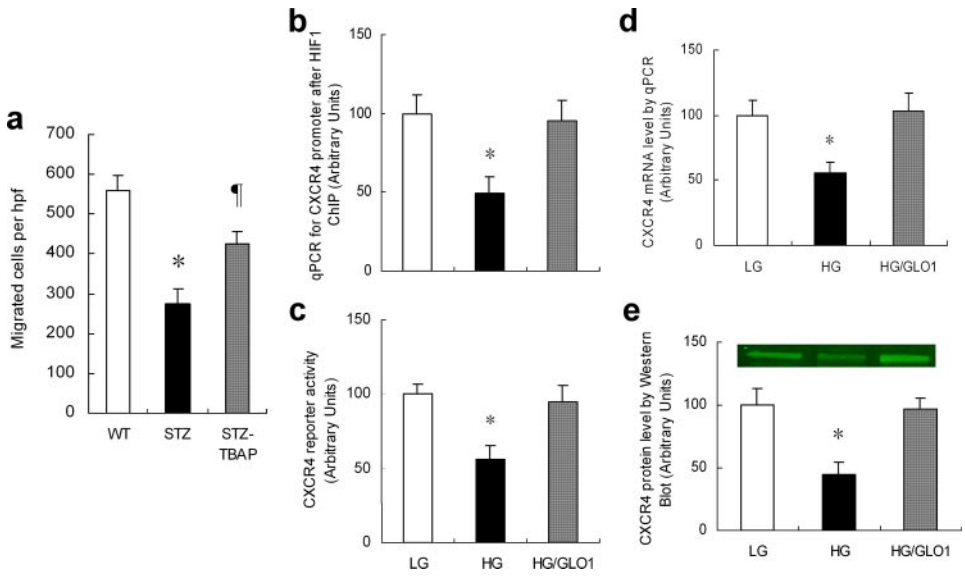

FIGURE 5. **Hyperglycemia-induced methylglyoxal modification of HIF-1α reduces CXCR4 expression in bone marrow-derived endothelial progenitor cells.** *a*, SDF-1 induced migration of Lin−/Sca-1+/c-Kit+ bone marrow progenitor cells harvested from WT, wild type diabetic (*STZ*), and wild type diabetic mice treated with an SOD mimetic (*STZ.TBAP*) (*, $p < 0.01$ *vs.* WT group; ¶, $p < 0.05$ *vs.* STZ group). *b–d*, bone marrow-derived murine EPCs were incubated in LG, HG, or HG after infection with ad-GLO1 (*HG/GLO1*) under hypoxic conditions. Treated cells were harvested and HIF-1α binding to the CXCR4 promoter was analyzed by ChIP (*b*), CXCR4 expression was analyzed using a CXCR4 Luc reporter (*c*) and by qPCR quantitation of CXCR4 mRNA (*d*). CXCR4 protein levels were measured by Western blotting using the ODYSSEY infrared imaging system (*e*). *, $p < 0.01$ *versus* LG group. Data are expressed as mean ± S.E., $n = 3$.

HIF-1α binding to the HRE-containing regions of both the SDF-1 (Fig. 4*c*) and the VEGF promoters (Fig. 4*d*). Together, these data show that hyperglycemia reduces the HIF-1-dependent transcription of SDF-1 and VEGF in response to hypoxia by methylgloxal modification of Arg^{17} and Arg^{23} in the bHLH domain of HIF-1α.

Superoxide-induced Methylglyoxal Modification of HIF1α by High Glucose in EPCs Causes Defective Transcription of the SDF1 Receptor and eNOS in Response to Hypoxia—After determining that hyperglycemia-induced methylglyoxal accumulation reduced the ability of ischemic tissue to generate appropriate levels of chemokine and growth factor signals, we next evaluated the effects of hyperglycemia on the ability of endothelial progenitor cells to respond to the ischemia-specific mobilizing signal SDF-1. Previous work has demonstrated that circulating progenitor cells from diabetic patients are functionally impaired (6). We first examined primitive Lin−/Sca-1+/c-Kit+ bone marrow progenitor cells from diabetic animals (19) and found a 40% increase in ROS compared with wild type animals (data not shown). *In vitro*, bone marrow progenitor cells from diabetic mice showed a marked impairment in their ability to migrate toward an SDF-1 gradient compared with non-diabetic controls (Fig. 5*a*), indicating that even in the presence of saturating amounts of this ischemia-specific EPC mobilizing chemokine, diabetic progenitor cells are intrinsically impaired. Progenitor cells from diabetic mice treated with Mn-TBAP had almost twice the migratory response of cells from untreated diabetic mice. Because expression of CXCR4, the SDF-1 receptor on EPCs, is also regulated by HIF-1, we then evaluated the effect of hyperglycemia-induced methylglyoxal modification of HIF-1α on CXCR4 expression. ChIP at the HRE of the *Cxcr4* promoter using DNA isolated from hypoxic EPCs showed that hyperglycemia decreased HIF-1α binding to the *Cxcr4* promoter by 50% (Fig. 5*b*). This was associated with a 50% decrease in CXCR4 reporter activity (Fig. 5*c*), mRNA (Fig. 5*d*), and protein level (Fig. 5*e*). Each of these effects of hyperglycemia was prevented by GLO1 overexpression (Fig. 5, *b–e*).

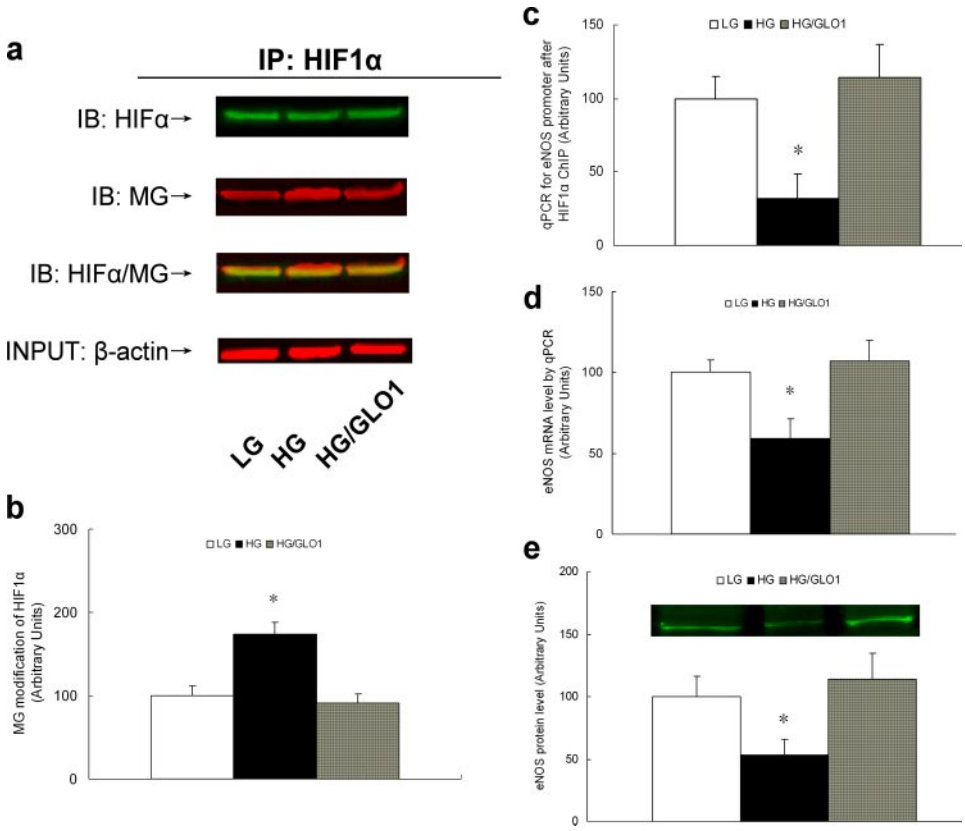

FIGURE 6. **Hyperglycemia-induced methylglyoxal modification of HIF-1α reduces eNOS expression in bone marrow-derived endothelial progenitor cells.** Bone marrow-derived murine EPCs were incubated in LG, HG, or HG after infection with ad GLO1 (HG/GLO1) under hypoxic conditions. *a*, nuclear extracts isolated from the above treated EPCs were immunoprecipitated (*IP*) with HIF-1α rabbit antibody and then immunoblotted (*IB*) with either HIF-1α antibody or a monoclonal antibody to the major intracellular methylglyoxal-derived epitope, *N*α-acetyl-*N*δ-(5-hydro-5-methyl)-4-imidazolone (*MG*). 10% of nuclear extracts were immunoblotted with β-actin antibody as input control. *b*, quantitation of methylglyoxal modification of HIF-1α in EPCs. *c*, HIF-1α binding to the eNOS promoter was analyzed by ChIP. *d*, treated cells were harvested and eNOS mRNA level was analyzed by real time qPCR. *e*, eNOS protein levels were measured by Western blotting using the ODYSSEY infrared imaging system. *, $p < 0.05$ *versus* LG group. Data are expressed as mean ± S.E., $n = 3$.

eNOS plays an essential role in EPC mobilization in a model of hindlimb ischemia and diabetic wound healing (5, 8). We previously reported that in normal oxygen, high glucose reduced eNOS activity by post-translational modification with *O*-linked *N*-acetylglucosamine at the Akt phosphorylation site (25). Gallagher *et al.* (5) found a similar decrease in eNOS phosphorylation at the Akt site in EPCs from diabetic mouse bone marrow, but did not investigate the effect of high glucose on eNOS expression during hypoxia. Because mouse eNOS, like human eNOS (26), contains an HRE element in the promoter (Ensembl Transcript ID ENST00000297494), we next evaluated the effect of hyperglycemia-induced methylglyoxal modification of HIF-1α on eNOS expression in response to hypoxia. HIF-1α modification by methylglyoxal was increased by hyperglycemia (Fig. 6, *a* and *b*). Concomitant ChIP at the HRE of the eNOS promoter using DNA isolated from hypoxic EPCs showed that hyperglycemia decreased HIF-1α binding to the *eNos* promoter by 68% (Fig. 6*c*). This was associated with a 41% decrease in *eNos* mRNA (Fig. 6*d*), and a 47%

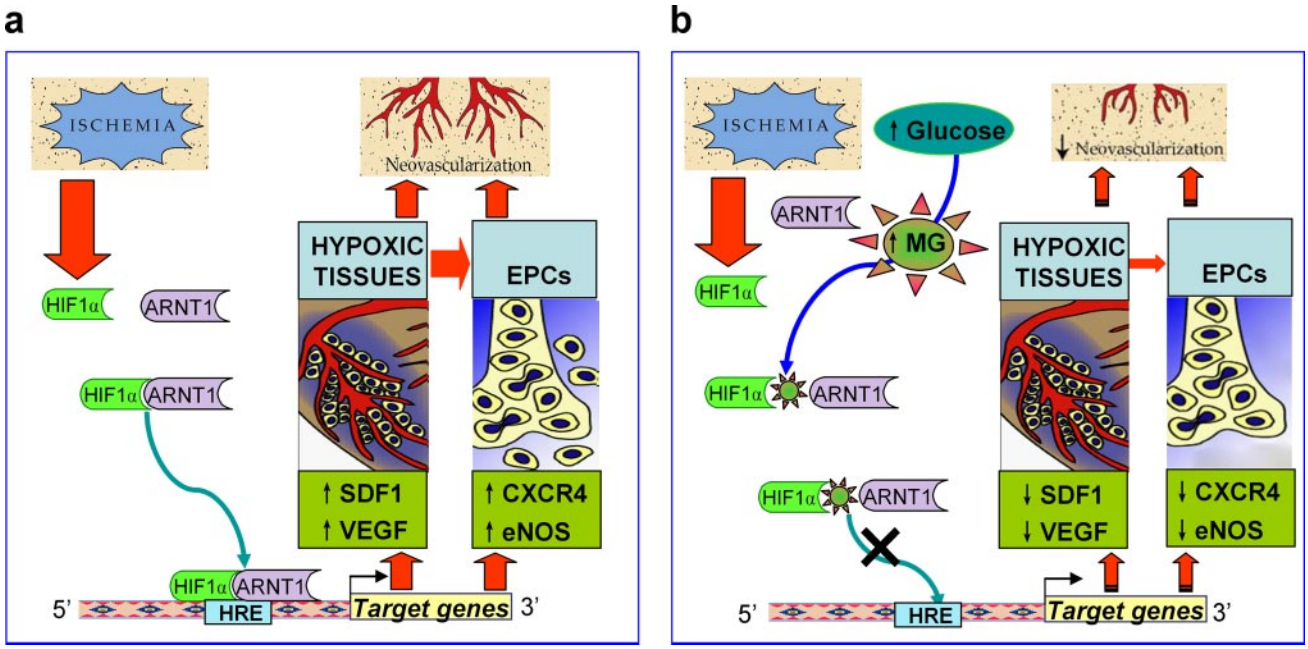

FIGURE 7. **Model of ischemia-induced neovascularization in normal and high glucose.** *a*, in the presence of normal glucose concentrations, ischemia-stabilized HIF1α forms heterodimers with ARNT1. These bind to HRE and activate expression of genes required for neovascularization. *b*, high glucose-induced MG modifies HIF1α, inhibiting heterodimer formation and binding to the HREs of genes required for neovascularization.

decrease in protein level (Fig. 6*e*). Each of these effects of hyperglycemia was prevented by GLO1 overexpression (Fig. 6, *a*–*e*). Together, these data indicate that hyperglycemia reduces hypoxic EPC CXCR4 and eNOS expression due to HIF-1α modification by methylglyoxal.

DISCUSSION

In the present study, we describe a shared molecular mechanism by which diabetic levels of high glucose reduce expression of genes critical to both the efferent and afferent limbs of ischemia-induced vasculogenesis: covalent modification of HIF1α by the glycolysis-derived metabolite dicarbonyl metabolite methylglyoxal (shown schematically in Fig. 7). Methylglyoxal levels increase in response to high levels of intracellular glucose because hyperglycemia causes an overproduction of superoxide by the mitochondrial electron transport system. This leads to activation of the nuclear enzyme poly(ADP-ribose) polymerase and subsequent inhibition of the glycolytic enzyme GAPDH by poly(ADP-ribosyl)ation. With GAPDH inhibited, the upstream triose phosphate glycolytic metabolites accumulate, producing more methylglyoxal (12).

We demonstrate that in hypoxic mouse fibroblasts, hyperglycemia causes increased modification of HIF1α at Arg-17 and Arg-23 of the bHLH domain, which reduces both heterodimer formation with ARNT and HIF1 binding to the promoters of *Sdf1* and *Vegf*. In hypoxic mouse EPCs, the same HIF1α modification reduces binding to the *Cxcr4* and *eNos* promoters. This HIF1α defect causes decreased mRNA and protein levels of all four gene products. Because eNOS activity in EPCs, which is critical for EPC mobilization, is reduced by two downstream consequences of hyperglycemia-induced ROS formation-increased methylglyoxal formation and increased flux through the hexosamine pathway (5, 12), we tested our hypothesis *in vivo* using *Mn-SOD* transgenic diabetic mice, and Mn-TBAP-treated mice, to prevent hyperglycemia-induced ROS. Both of these interventions prevented diabetes-induced post-ischemic defects in neovascularization, oxygen delivery, and chemokine expression, and normalized tissue survival. Because transgenic changes in gene expression during development could, in theory, cause compensatory changes that affect the adult phenotype, it is important to note that treatment of adult diabetic mice with an SOD mimetic had qualitatively identical effects on ischemia-induced vasculogenesis. Modification of transcription factor function by post-transcriptional modification has been well described. Of particular interest in the context of diabetes is modification by *O*-linked *N*-acetylglucosamine (27, 28). Modification of coregulatory proteins has also been described, including both coactivators (29, 30) and the corepressor mSin3A (14). The latter is particularly germane to diabetes, because hyperglycemia-induced ROS cause increased methylglyoxal modification of mSin3A, with resultant alterations in function. Our finding that hyperglycemia-induced superoxide decreases HIF-1 function by increasing HIF-1α modification by the glucose-derived α-oxoaldehyde methylglyoxal has important clinical implications. Because decreased HIF-1 function impairs both ischemic cell signaling and the bone marrow-derived endothelial cell precursor response, impaired vasculogenesis in people with diabetes contributes to increased mortality rates after myocardial infarction, and increased rates of lower limb amputation. Thus, the dramatic improvement of ischemic tissue revascularization and survival in diabetic animal models by transgenically expressed SOD and SOD mimetics has great relevance for drug design and future clinical trials.

REFERENCES

1. Abaci, A., Oguzhan, A., Kahraman, S., Eryol, N. K., Unal, S., Arinc, H., and Ergin, A. (1999) *Circulation* **99,** 2239–2242
2. Yarom, R., Zirkin, H., Stammler, G., and Rose, A. G. (1992) *J. Pathol.* **166,** 265–270
3. Rivard, A., Silver, M., Chen, D., Kearney, M., Magner, M., Annex, B., Peters, K., and Isner, J. M. (1999) *Am. J. Pathol.* **154,** 355–363
4. Schatteman, G. C., Hanlon, H. D., Jiao, C., Dodds, S. G., and Christy, B. A. (2000) *J. Clin. Investig.* **106,** 571–578
5. Gallagher, K. A., Liu, Z. J., Xiao, M., Chen, H., Goldstein, L. J., Buerk, D. G., Nedeau, A., Thom, S. R., and Velazquez, O. C. (2007) *J. Clin. Investig.* **117,** 1249–1259
6. Tepper, O., Galiano, R., Capla, J., Kalka, C., Gagne, P., Jacobowitz, G., Levine, J., and Gurtner, G. (2002) *Circulation* **106,** 2781–2786
7. Asahara, T., Takahashi, T., Masuda, H., Kalka, C., Chen, D., Iwaguro, H., Inai, Y., Silver, M., and Isner, J. M. (1999) *EMBO J.* **18,** 3964–3972
8. Aicher, A., Heeschen, C., Mildner-Rihm, C., Urbich, C., Ihling, C., Technau-Ihling, K., Zeiher, A. M., and Dimmeler, S. (2003) *Nat. Med.* **9,** 1370–1376
9. Ceradini, D. J., Kulkarni, A. R., Callaghan, M. J., Tepper, O. M., Bastidas, N., Kleinman, M. E., Capla, J. M., Galiano, R. D., Levine, J. P., and Gurtner, G. C. (2004) *Nat. Med.* **10,** 858–864
10. Ceradini, D. J., and Gurtner, G. C. (2005) *Trends Cardiovasc. Med.* **15,** 57–63
11. Kaelin, W. G. (2005) *Annu. Rev. Biochem.* **74,** 115–128
12. Brownlee, M. (2001) *Nature* **414,** 813–820
13. Galasso, G., Schiekofer, S., Sato, K., Shibata, R., Handy, D. E., Ouchi, N., Leopold, J. A., Loscalzo, J., and Walsh, K. (2006) *Circ. Res.* **98,** 254–261
14. Yao, D., Taguchi, T., Matsumura, T., Pestell, R., Edelstein, D., Giardino, I., Suske, G., Rabbani, N., Thornalley, P. J., Sarthy, V. P., Hammes, H. P., and Brownlee, M. (2007) *J. Biol. Chem.* **282,** 31038–31045
15. Tepper, O. M., Capla, J. M., Galiano, R. D., Ceradini, D. J., Callaghan, M. J., Kleinman, M. E., and Gurtner, G. C. (2005) *Blood* **105,** 1068–1077
16. Dimmeler, S., Aicher, A., Vasa, M., Mildner-Rihm, C., Adler, K., Tiemann, M., Rütten, H., Fichtlscherer, S., Martin, H., and Zeiher, A. (2001) *J. Clin. Investig.* **108,** 391–397
17. Metivier, R., Penot, G., Hubner, M. R., Reid, G., Brand, H., Kos, M., and Gannon, F. (2003) *Cell* **115,** 751–763
18. Asahara, T., Murohara, T., Sullivan, A., Silver, M., van der Zee, R., Li, T., Witzenbichler, B., Schatteman, G., and Isner, J. (1997) *Science* **275,** 964–967
19. Awad, O., Jiao, C., Ma, N., Dunnwald, M., and Schatteman, G. C. (2005) *Stem Cells* **23,** 575–583
20. Suri, C., Jones, P. F., Patan, S., Bartunkova, S., Maisonpierre, P. C., Davis, S., Sato, T. N., and Yancopoulos, G. D. (1996) *Cell* **87,** 1171–1180
21. Ahmed, N., and Thornalley, P. J. (2003) *Biochem. Soc. Trans.* **31,** 1417–1422
22. Ahmed, N., Argirov, O. K., Minhas, H. S., Cordeiro, C. A., and Thornalley, P. J. (2002) *Biochem. J.* **364,** 1–14
23. Ahmed, N., Dobler, D., Dean, M., and Thornalley, P. J. (2005) *J. Biol. Chem.* **280,** 5724–5732
24. Michel, G., Minet, E., Mottet, D., Remacle, J., and Michiels, C. (2002) *Biochim. Biophys. Acta* **1578,** 73–83
25. Du, X. L., Edelstein, D., Dimmeler, S., Ju, Q., Sui, C., and Brownlee, M. (2001) *J. Clin. Investig.* **108,** 1341–1348
26. Coulet, F., Nadaud, S., Agrapart, M., and Soubrier, F. (2003) *J. Biol. Chem.* **278,** 46230–46240
27. Hart, G. W., Housley, M. P., and Slawson, C. (2007) *Nature* **446,** 1017–1022
28. Comer, F. I., and Hart, G. W. (2000) *J. Biol. Chem.* **275,** 29179–29182
29. Fingerman, I. M., and Briggs, S. D. (2004) *Cell* **117,** 690–691
30. Chakraborty, S., Senyuk, V., and Nucifora, G. (2001) *J. Cell. Biochem.* **82,** 310–325